



HAL
open science

Synthesis of a Negative Photochrome with High Switching Quantum Yields and Capable of Singlet-Oxygen Production and Storage

Zakaria F Ziani, Frédérique Loiseau, Elise Lognon, Martial Boggio-Pasqua, Christian Philouze, Saioa Cobo, Guy Royal

► **To cite this version:**

Zakaria F Ziani, Frédérique Loiseau, Elise Lognon, Martial Boggio-Pasqua, Christian Philouze, et al.. Synthesis of a Negative Photochrome with High Switching Quantum Yields and Capable of Singlet-Oxygen Production and Storage. *Chemistry - A European Journal*, 2021, 27 (67), pp.16642-16653. 10.1002/chem.202103003 . hal-03421341

HAL Id: hal-03421341

<https://hal.science/hal-03421341>

Submitted on 9 Nov 2021

HAL is a multi-disciplinary open access archive for the deposit and dissemination of scientific research documents, whether they are published or not. The documents may come from teaching and research institutions in France or abroad, or from public or private research centers.

L'archive ouverte pluridisciplinaire **HAL**, est destinée au dépôt et à la diffusion de documents scientifiques de niveau recherche, publiés ou non, émanant des établissements d'enseignement et de recherche français ou étrangers, des laboratoires publics ou privés.

Synthesis of a Negative Photochrome with High Switching Quantum Yields and Capable of Singlet Oxygen Production and Storage

Zakaria Ziani,^[a] Frédérique Loiseau,^[a] Elise Lognon,^[b] Martial Boggio-Pasqua,^{* [b]} Christian Philouze,^[a] Saïoa Cobo,^[a] and Guy Royal,^{* [a]}

[a] Z. Ziani, Prof. F. Loiseau, Dr. C. Philouze, Dr. S. Cobo, Prof. G. Royal
Univ. Grenoble-Alpes, CNRS, Département de Chimie Moléculaire
F-38400 Grenoble (France)

E-mail: guy.royal@univ-grenoble-alpes.fr

[b] E. Lognon, Dr. M. Boggio-Pasqua
LCPQ UMR 5626, CNRS et Université Toulouse III – Paul Sabatier
118 route de Narbonne, 31062 Toulouse (France)
E-mail: martial.boggio@irsamc.ups-tlse.fr

Supporting information for this article is given via a link at the end of the document.

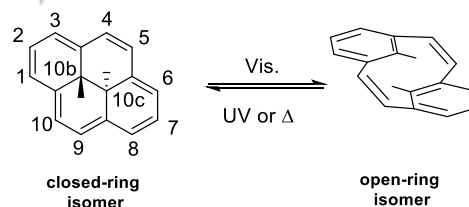
Abstract: A dimethyldihydropyrene (DHP) photochromic unit has been functionalized by donor (triphenylamine group) and acceptor (methyl-pyridinium) substituents. This compound was characterized by NMR, absorption and emission spectroscopies as well as cyclic voltammetry and its properties were rationalized by theoretical calculations. The incorporation of both electron donor and withdrawing groups on the photochromic center allows *i)* an efficient photo-isomerization of the system when illuminated at low energy (quantum yield: $\Phi_{c-o} = 13.3\%$ at $\lambda_{ex.} = 660$ nm), *ii)* the reversible and quantitative formation of two endoperoxide isomers when illuminated under aerobic conditions at room temperature and *iii)* the storage and production of singlet oxygen. The photo-isomerization mechanism was also investigated by spin-flip TD-DFT (SF-TD-DFT) calculations.

Introduction

Organic photochromic molecules,^[1–5] such as the well-known spiropyranes, dithienylethenes, azobenzenes or the more recently developed DASA (donor–acceptor Stenhouse adducts) derivatives can be reversibly converted between (at least) two isomeric forms on exposure to light of different wavelengths and these isomers may exhibit distinct properties such as polarisability, luminescence, solubility, shape or conductivity. These photochroms can thus play the role of active components in numerous applications^[6] such as optical imaging, materials science, energy (photovoltaic cells, light emitting diodes...), or medical purposes (diagnostic, therapy...)^[7–9] However, for most of these domains, and in particular in the field of biology, the use of ultraviolet (UV) light as input must be avoided due to its high energy that can cause damages and because of its short penetration length in tissues. It is thus essential to develop photoswitches that can be triggered by illumination within the biological window (mainly $\lambda = 650–1000$ nm).^[10]

In this context, the development of the dimethyldihydropyrene (trans-10b,10c-dimethyl-10b,10c-dihydropyrene, **DHP**, closed isomer, see Scheme 1) photochromic unit is of particular interest. Indeed, this colored and aromatic compound (14 delocalized π

electrons)^[11,12] belongs to the uncommon class of negative photochroms, *i.e.* the conversion between the colored and thermodynamically stable **DHP** to the colorless cyclophanediene (**CPD**, open form) isomer is triggered by visible light. In addition, the reversion of the metastable **CPD** form to the stable **DHP** can be quantitatively realized either by illumination with UV light or thermally (T-type).



Scheme 1. Schematics of the dimethyldihydropyrene (left) / cyclophanediene (right) photochromic couple.

Another major asset of the **DHP** core is that its structure can be regarded as a real molecular platform that can be readily modified chemically in order to adapt and tune its properties towards the targeted applications. For example, functionalization of the **DHP** unit by metal complexes may lead to all-visible light switches^[10] and the incorporation of both donor and acceptor substituents (push-pull systems) was recently shown to promote efficient **DHP** to **CPD** photoconversions triggered by NIR light ($\lambda > 800$ nm).^[13,14] In addition, we have previously reported that the suitable functionalization of the DHP moiety with pyridinium substituent(s) has two effects: *i)* the quantum yield of the ring-opening conversion (**DHP** to **CPD**) may be significantly increased (by ~2 orders)^[15,16] and *ii)* the system may display an unusual reactivity towards dioxygen: the closed-ring isomer can play the role of O_2 photosensitizer (photo-production of singlet oxygen) and may also quantitatively and reversibly generate endoperoxide derivatives when illuminated by red light under aerobic conditions.^[17,18] Following these results, we describe herein the preparation and characterization of a new donor-acceptor **DHP**

derivative (**DA-DHP**, Chart 1) bearing both an electro-acceptor pyridinium group and an electron-donor triphenylamine unit. The physico-chemical and photochromic properties of this compound are investigated as well as its reactivity under aerobic conditions. Related compounds (**DHP**, **A-DHP**, **D-DHP**, Chart 1) are also studied for comparison.

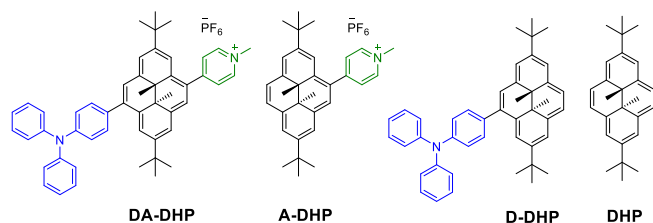
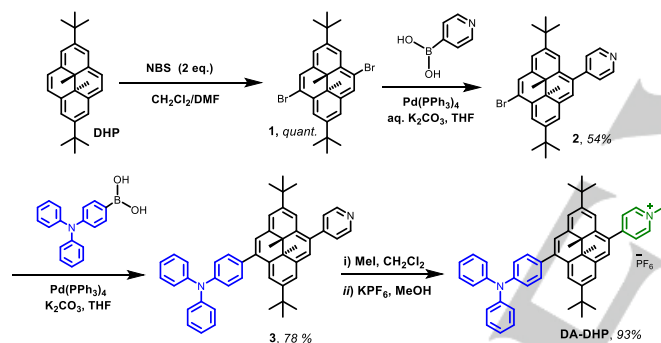


Chart 1. Investigated Donor-Acceptor dimethyldihydropyrene photochromic compound (**DA-DHP**) and reference molecules investigated in this work.

Results and Discussion

Synthesis

The investigated **DA-DHP** system was prepared following the synthetic route represented in Scheme 2.



Scheme 2. Synthetic procedure for the preparation of **DA-DHP**.

The procedure starts with the 2,7-di-*t*-butyl-trans-10b,10c-dimethyl-10b,10c-dihydropyrene (**DHP**) which was first brominated in positions 4 and 9 by reaction with 2 molar equivalents of *N*-bromosuccinimide (NBS) in DMF and CH_2Cl_2 as solvents (the *tert*-butyl groups were incorporated for solubility and synthetic reasons).^[11] In order to introduce different substituents on the DHP core, the bis-brominated compound **1** was subjected to two consecutive Suzuki-Miyaura coupling reactions in the presence of tetrakis-triphenylphosphine palladium as catalyst. The first coupling was done with 1 molar equivalent of 4-pyridylboronic acid and compound **2** was isolated with 54% yield. Then, coupling between **2** and 1.3 equivalent of triphenylamine-4-boronic acid yielded **3** which was isolated as an orange powder (yield: 78%). This latter was then reacted with an excess of methyl iodide and the crude reaction product was subjected to an anion exchange procedure to afford the targeted red **DA-DHP** which was isolated as its PF_6^- salt. Reference molecules containing only one acceptor (**A-DHP**) or donor (**D-DHP**) group (see Chart 1) were prepared following similar experimental protocols by coupling the mono-brominated **DHP** with the corresponding

pyridine or triphenylamine boronic derivatives, respectively (see experimental section).

Characterization of DA-DHP and related compounds

The synthesized compounds investigated in this work were analyzed by UV/vis absorption and ^1H and ^{13}C NMR spectroscopies as well as mass spectrometry measurements (see experimental section and S.I.). In particular, the ^1H NMR spectrum of **DA-DHP**, recorded in CD_3CN , is shown in Figure 1 and confirms the formation of the targeted compound. Signals observed at low field (7–9 ppm) were attributed to the resonance of the hydrogen atoms of the **DHP** core and the pyridine and triphenylamine units. The singlet signals corresponding to the $\text{N}^+\text{-CH}_3$ groups and to the *t*-Bu units appear at +4.40 and \sim +1.6 (2 singlets) ppm, respectively. In contrast, peaks of the internal methylenic protons are found in the negative region of the spectrum, at -3.65 and -3.67 ppm. The unusual position of these signals is due to the ring current flowing through the delocalized π -electrons of the **DHP** core and constitutes thus a real signature indicating that the photochromic unit is in its closed state.^[11] The structures of the other compounds investigated in this work were similarly confirmed by NMR studies (see S.I. and experimental section).

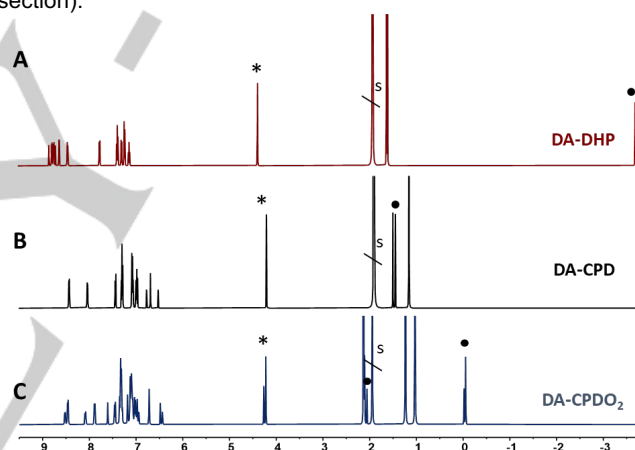


Figure 1. ^1H -NMR of (A) **DA-DHP**, (B) **DA-CPD** and (C) **DA-CPDO**₂ in CD_3CN . • and * indicate the signals of the internal methyl and $\text{N}^+\text{-CH}_3$ groups, respectively. s: solvent peak

The structure of **D-DHP** has also been confirmed via single crystal X-ray diffraction analyses (see Figure S19). This compound crystallizes in the space group P-1 (triclinic system). The sp^2 carbon atoms of the DHP core are planar and the distance measured between the two central sp^3 carbon atoms is 1.52 Å, which is similar to values found for other DHP derivatives^[16] and in agreement with the gas phase optimized structure using DFT at 1.54 Å. The phenyl group of the triphenylamine unit directly connected to the DHP adopts a dihedral angle of 47.1° with respect to the main DHP plane, close to the gas phase optimized structure which gives a slightly larger dihedral angle of 52.9°. The investigated compounds were analyzed by UV/vis absorption spectroscopy associated to theoretical calculations. Experimental absorption spectra are given in Figure 2 and corresponding data are collected in Table 1. Vertical transition energies computed with TD-DFT are reported in Table 2 for comparison and Table 3 illustrates the nature of the lowest two electronic transitions involved for each system.

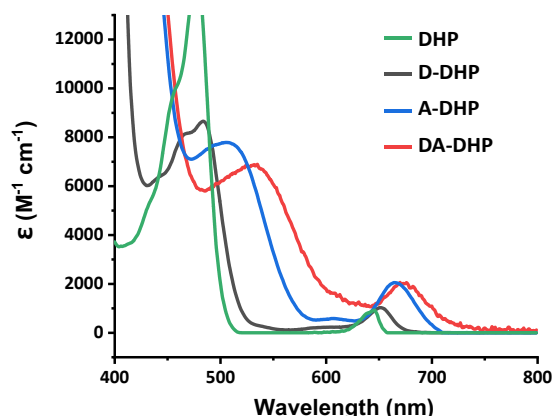


Figure 2. UV/vis spectra of **DHP** (green line), **D-DHP** (black line), **A-DHP** (blue line) and **DA-DHP** (red line). Solvents used: cyclohexane for **DHP** and **D-DHP**; acetonitrile for **A-DHP** and **DA-DHP**.

Table 1. Absorption data and quantum yields for the photo-ring opening process (Φ_{c-o}) for the **DHP**, **A-DHP**, **D-DHP** and **DA-DHP** compounds.^[a]

Compounds	Absorption λ , nm ($\epsilon/10^4$ M ⁻¹ cm ⁻¹)	Quantum yields Φ_{c-o} (λ / nm) ^[b]
DHP ^[19]	641 (0.09), 477 (1.1), 379 (3.9), 341 (10.3)	0.00% (660) 0.08% (470)
A-DHP ^[16]	666 (0.2), 510 (0.7), 416 (2.4), 337 (5.2), 251 (1.3)	9.30% (660)
D-DHP	652 (0.1), 484 (0.8), 470 (0.8), 395 (4.5), 348 (4.8)	0.00% (660) 0.01% (470)
DA-DHP	676 (0.2), 535 (0.6), 422 (1.8), 341 (2.7), 304 (2.2)	13.3% (660)

[a] For solubility reasons, **DHP** and **D-DHP** were studied in cyclohexane and **A-DHP** and **DA-DHP** were investigated in acetonitrile. [b] Values indicated in parentheses correspond to wavelengths used for both excitation and detection during quantum yields measurements.

In the 300-800 nm range, the absorption spectrum of **DHP** exhibits main bands attributed to $\pi-\pi^*$ transitions that involve singlet electronic states of the chromophore core.^[20] In **D-DHP**, these absorption bands appear red-shifted, in accordance with an extension of the π -system and this bathochromic shift is nicely reproduced by the TD-DFT calculations (Table 2). Note that the two bands observed experimentally at 484 nm and 470 nm result from the same electronic transition according to the TD-DFT calculations, and are thus the results of vibronic structures. In the case of **A-DHP**, the shifts of the absorption bands towards lower energies are even more pronounced and it is important to note that the extinction coefficient of the band at lowest energy is also significantly increased. These observations are supported by the TD-DFT results (Table 2). As explained in a previous study,^[16] these effects are partially due to the charge transfer character between the **DHP** moiety and the methyl-pyridinium unit, which is illustrated by the pair of NTOs associated with these electronic transitions (Table 3). In the case of **DA-DHP**, which contains both pyridinium and the donor amino group, no intramolecular charge-transfer (ICT) excitation from the electron donor group to the electron acceptor moiety has been observed (see NTOs for S_1

and S_2 states of **DA-DHP** in Table 3). However, the absorption spectrum is clearly the most red-shifted among the investigated compounds (see Figure 2). In particular, the absorption peak appearing at lowest energy ($S_0 \rightarrow S_1$ transition) is located at 641 nm in the simple **DHP** and is found at 676 nm in **DA-DHP**, which corresponds to a shift of -0.106 eV in energy. This experimental value is thus in reasonable agreement with an energy shift of -0.131 eV obtained from TD-DFT data.

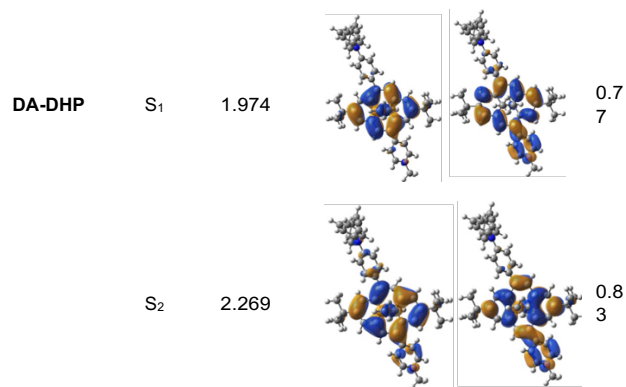
Table 2. Vertical transitions computed for the **DHP**, **A-DHP**, **D-DHP** and **DA-DHP** at the TD- ω B97X-D/6-311G(d,p) level..

Compounds	Vertical transitions ^[a] λ , nm ($f^{[b]}$)
DHP	589 (0.009), 503 (0.090), 378 (0.333), 340 (1.419)
A-DHP	620 (0.047), 529 (0.069), 413 (0.715), 379 (0.290), 344 (0.471), 309 (0.448)
D-DHP	600 (0.017), 511 (0.075), 392 (0.660), 349 (1.348)
DA-DHP	628 (0.073), 547 (0.144), 422 (1.088), 382 (0.266), 352 (0.306), 323 (0.362), 308 (0.174)

[a] Transitions above 300 nm are reported. [b] Oscillator strength.

Table 3. Comparison of the first two electronic transitions in **DHP**, **A-DHP**, **D-DHP** and **DA-DHP**.^[a]

Compound	State	Excitation Energy (eV)	NTOs ^[a]	κ ^[b]
DHP	S_1	2.103		0.68
	S_2	2.467		0.84
A-DHP	S_1	2.000		0.76
	S_2	2.343		0.81
D-DHP	S_1	2.067		0.68
	S_2	2.425		0.83



[a] Main pair of natural transition orbitals (with $\kappa > 0.5$) reflecting the dominant particle-hole excitation character obtained at TD- ω B97X-D/6-311G(d,p) level. [b] Largest natural transition orbital eigenvalue (κ) for each state.

The redox properties of the derivatives were characterized by cyclic voltammetry (CV) experiments conducted in CH_3CN (charged compounds) or CH_2Cl_2 (neutral molecules) solutions containing tetra-*n*-butylammonium hexafluorophosphate (TBAPF_6) as supporting electrolyte. Electrochemical data are summarized in Table 4. For all CV curves, in addition to oxidation (DHP^+/DHP and $\text{DHP}^{2+}/\text{DHP}^+$ couples) and reduction (DHP/DHP^-) processes centered on the DHP unit, reduction of the pyridinium centers (Py/Py^-) and/or oxidation waves of the triphenylamine group (TPA^+/TPA) were also logically observed with the substituted compounds. Potential shifts measured for the redox systems centered on the DHP moiety were in full accordance with the electronic effects of the donor and acceptor groups. However, when comparing the effects of the methyl-pyridinium (**A**) and TPA (**D**) substituents, it should be outlined that the major impacts are due to the presence of the pyridinium group. In particular, a decay of +140 mV was observed for $E_{1/2}$ (DHP^+/DHP) upon introduction of the pyridinium group to the DHP core (in **A-DHP**), whereas a shift of only -20 mV was seen in **D-DHP** (Table 4). In the same manner, the potential corresponding to the first oxidation of the DHP core in **DA-DHP** is positively shifted compared to the signal of the unsubstituted photochrome, showing that the acceptor group plays a larger electronic effect than the donor group. Such minor influence of the donor unit may be explained by the non-coplanarity between the triphenylamine unit and the main plane of the DHP moiety (as shown above, a dihedral angle of 47.1 was observed at the solid state with **D-DHP**; see Figure S19).

Table 4. Electrochemical data: oxidation and reduction potentials ($E_{1/2}$ (ΔE_p)^a, V) measured by cyclic voltammetry.

	DHP/ DHP ⁻	Py ⁺ / Py	DHP ⁺ / DHP	TPA ⁺ / TPA	DHP ²⁺ / DHP ⁺
DHP ^[c]	-2.35 (0.07)	—	0.19 (0.07)	—	$E_{pa} = 0.77$ ^[e]
A-DHP ^[d]	$E_{pc} = -$ 1.98 ^[e]	-1.36 (0.07)	0.33 (0.07)	—	$E_{pa} = 0.82$ ^[e]
D-DHP ^[c]	[f]	—	0.17 (0.08)	0.52 (0.08)	1.00 (0.10) ^[d]
DA-DHP ^[d]	-1.97 (0.07)	-1.45 (0.07)	0.27 (0.07)	0.52 (0.07) ^[d]	0.75 (0.08)

[a] E (V) vs. $E_{1/2}$ (ferrocenium/ferrocene); [b] $E_{1/2} = (E_p^a + E_p^c)/2$ at 0.1 V s^{-1} ; $\Delta E_p = E_p^a - E_p^c$; [c] in CH_2Cl_2 + 0.2 M TBAPF_6 ; [d] in CH_3CN + 0.1M TBAPF_6 ; [e] non-fully reversible system; [f] peak potential / irreversible system; [f] not observed in the measured potential range.

Study of the photo-ring opening process by illumination under inert atmosphere ($\text{DHP} \rightarrow \text{CPD}$)

Conversions of the closed-ring (DHP) isomers to their corresponding open-ring (CPD) forms were realized by irradiation with visible light and were followed by ^1H NMR and absorption spectroscopies. For these experiments, deaerated solutions of the different compounds ($\sim 10^{-3}$ and 10^{-6} M for NMR and UV/vis absorption spectroscopy, respectively) were cooled at 4°C during the entire irradiation period in order to avoid a possible thermal return reaction. Solutions were analysed at regular time intervals until no more changes in the spectra were observed.

In the case of **DA-DHP**, the photochemical conversion to **DA-CPD** was found to be effective when the solution was irradiated at $\lambda_{\text{ex}} \geq 630 \text{ nm}$ (using a high-pass filter) which corresponds to absorption on the lowest energy band of the compound (S_0 to S_1 transition). Figure 3 shows the evolution of the UV/vis spectra during the photo-conversion process.

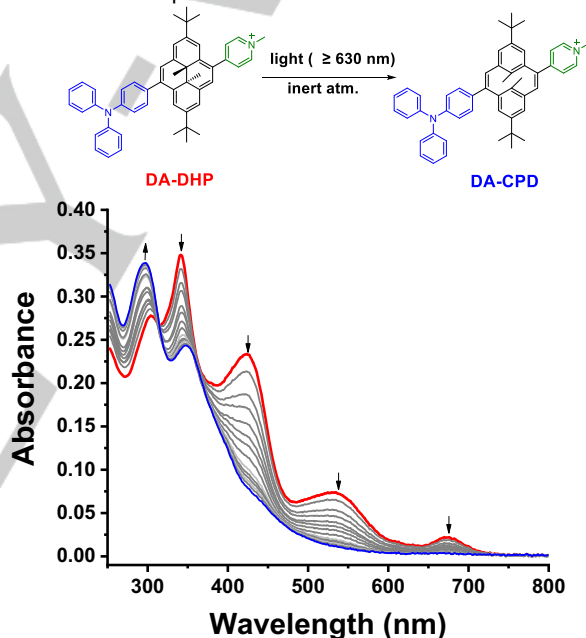


Figure 3. Top: isomerization of **DA-DHP** to **DA-CPD** by irradiation. Below: UV/vis absorption spectra evolution during irradiation ($\lambda_{\text{ex}} \geq 630 \text{ nm}$, 4°C) of **DA-DHP** in CH_3CN under inert atmosphere. Time between two consecutive spectra: 2 min.

During illumination, a rapid colour change from red to light yellow was observed, in agreement with the **DA-DHP** to **DA-CPD** conversion. This result is reflected by a disappearance of the visible absorption bands accompanied by the growth of the signal in the UV part of the spectrum and the presence of an isosbestic point at 313 nm. In the same manner, ^1H NMR peaks of **DA-DHP** were progressively replaced by new sets of resonance of the corresponding open-ring isomer **DA-CPD** during illumination (see Figure 1B). In particular, the two singlets of the internal methyl groups were considerably shifted from -3.6 ppm in the closed isomer to +1.5 ppm in the open form. At the end of the experiment,

no peak of the closed-ring isomer could be detected, showing a quantitative photo-conversion, at the NMR scale.

In contrast, no conversion was observed when **DHP** or **D-DHP** were irradiated under the same conditions (at $\lambda_{\text{ex}} \geq 630$ nm) and only a slow conversion was seen when these compounds were illuminated at $\lambda_{\text{ex}} = 470$ nm. In accordance with our previous results,^[15,16] this difference is attributed to the fact that, when a pyridinium group is introduced, excitation of the system to its lowest excited electronic state (S_1 level) may lead to the photo-ring opening reaction, whereas higher excitation levels must be reached to isomerize **DHP** or **D-DHP** into their open forms. In order to illustrate the effects of the chemical substitutions of the DHP core, solutions of **DHP**, **D-DHP**, **A-DHP** and **DA-DHP** were illuminated at $\lambda_{\text{ex}} \geq 700$ nm and the consumptions of the closed form were followed by UV/vis spectroscopy. As shown in Figure 4, under these experimental conditions, only **A-DHP** and **DA-DHP** could be logically converted to their open-ring isomers and the higher rate of conversion was clearly obtained with **DA-DHP**. For example, upon 1 hour of irradiation, more than 95 % of **DA-CPD** were formed whereas 25% of **A-DHP** were still remaining and no **CPD** or **D-CPD** were detected.

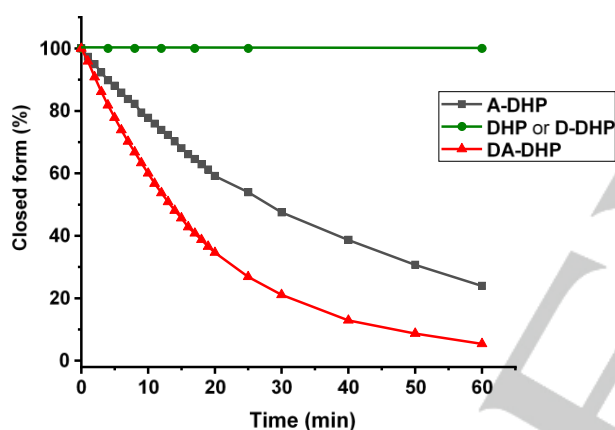


Figure 4. Percentage of **DHP**, **D-DHP**, **A-DHP** and **DA-DHP** closed-ring isomers measured during illumination at $\lambda_{\text{ex}} \geq 700$ nm as function of time. The amount of the closed form is determined by the absorbance at the maximum wavelengths. [C] = 10^{-5} M in CH_3CN (**A-DHP** and **DA-DHP**) or cyclohexane (**DHP**, **D-DHP**).

The efficiency of the photo-controlled reaction from closed to open-ring isomers was quantified by the determination of their quantum yields ($\Phi_{\text{c-o}}$) which represent the number of CPD molecules produced per photon absorbed. For this, 10^{-6} to 10^{-5} M solutions of closed isomers were irradiated at specific wavelengths and the conversion was followed by absorption spectroscopy. Quantum yields were then determined by fitting the results using the kinetic model reported by Maaft and Brown.^[21,22] The $\Phi_{\text{c-o}}$ values are collected in Table 1. Whereas the **DHP** and **D-DHP** compounds exhibit low quantum yields (<0.1%) when irradiated at 470 nm and could not be isomerized at 660 nm, values of 9.3% and 13.3% were found in **A-DHP** and **DA-DHP**, respectively when illuminated at low energy ($\lambda_{\text{ex}} = 660$ nm). Such increase of the quantum yield between **DA-DHP** and **A-DHP** (+43%) confirms the major positive effect played by the introduction of both the electron-withdrawing pyridinium and the

electron-donor triphenylamine groups on the dimethyldihydropyrene skeleton.

In order to investigate the photo-isomerization mechanism on the lowest S_1 excited state of the **DA-DHP** system, we report for the first time the excited-state relaxation pathway from the Franck-Condon region to the photochemical funnel, that is the S_0/S_1 conical intersection, responsible for the nonradiative decay down to S_0 on the way to the CPD photoproduct formation. The photo-isomerization pathway is illustrated in Figure 5 based on SF-TD-DFT calculations.^[23–26] Our results show that upon initial relaxation from the Franck-Condon region, the system reaches a minimum, **DA-DHP***, on the S_1 potential energy surface. The associated relaxation coordinate involves mainly some C-C skeletal deformation of the DHP core (see Figure S20). To reach the minimum energy conical intersection (*i.e.*, the lowest energy crossing between S_1 and S_0), **S_0/S_1 MECI**, the system needs to undergo a loss of planarity associated with an increased transannular C-C bond length and a reorientation of the pyridinium group (see Figure S20). This process is activated and the S_1 transition state optimized (at the TD-DFT level; see Computational Details) along this relaxation path provides an estimated S_1 potential energy barrier of 6.3 kcal/mol (0.272 eV). The **S_0/S_1 MECI** is energetically accessible, lying 4.1 kcal/mol (0.180 eV) above **DA-DHP*** and only 2.0 kcal/mol (0.087 eV) above the Franck-Condon energy. The main difference with the reference **DHP** system is that the S_1 state of **DA-DHP** can lead to photoisomerization, whereas this is not the case in **DHP**. In the parent **DHP**, the system needs to be excited in S_2 and the low photoisomerization quantum yield is due to an efficient depopulation of S_2 towards S_1 , which is unreactive.^[24,25] The present mechanism will thus lead to a much more efficient photoisomerization in **DA-DHP** compared to the reference compound **DHP**.

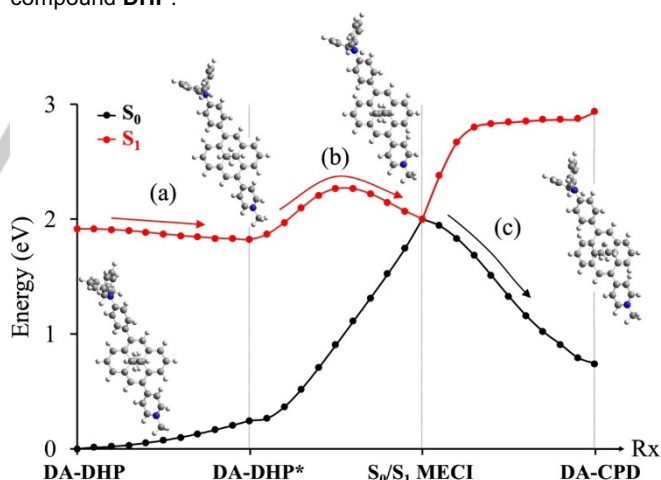


Figure 5. Photo-isomerization pathway from ground-state **DA-DHP** to **DA-CPD**: (a) excited-state relaxation on S_1 to **DA-DHP***, (b) activated process to reach the photochemical funnel (S_0/S_1 MECI), and (c) nonradiative deactivation to S_0 and ground-state relaxation to **DA-CPD**. All the molecular structures and Cartesian coordinates are provided in SI.

Investigation of the optically and thermally triggered ring-closing reaction (**CPD**→**DHP**)

As seen previously, the ring-closure reaction, *i.e.* the CPD to DHP conversion, can generally be achieved by UV illumination or by heating. When a solution of **DA-CPD** (freshly prepared by visible

FULL PAPER

irradiation of a solution of **DA-DHP**) was exposed to UV light (254 nm or 366 nm, 7W), a change of colour was rapidly observed and the reaction could be followed by ^1H NMR and UV/vis absorption spectroscopies. Spectra of the initial **DA-DHP** could be regenerated upon few seconds of illumination without any observable degradation, showing the efficient optically-controlled ring-closing process.

In the same manner and in order to evaluate the thermal return reaction, CH_3CN solutions of **DA-CPD** were heated under dark conditions and the closed-ring isomer could be progressively and quantitatively generated (see Figures S6, S10 and S11). Different temperatures were used and, assuming a first order kinetic, an activation energy E_a of $22.4 \pm 2.1 \text{ kcal}\cdot\text{mol}^{-1}$ was measured. This value is in accordance with DFT calculations for which an activation energy of 19.4 kcal/mol was found and is similar to most CPD derivatives reported in the literature.^[27] In addition, a half lifetime ($t_{1/2}$) of $69 \pm 2 \text{ min}$ was found for **DA-DHP** at 37°C .

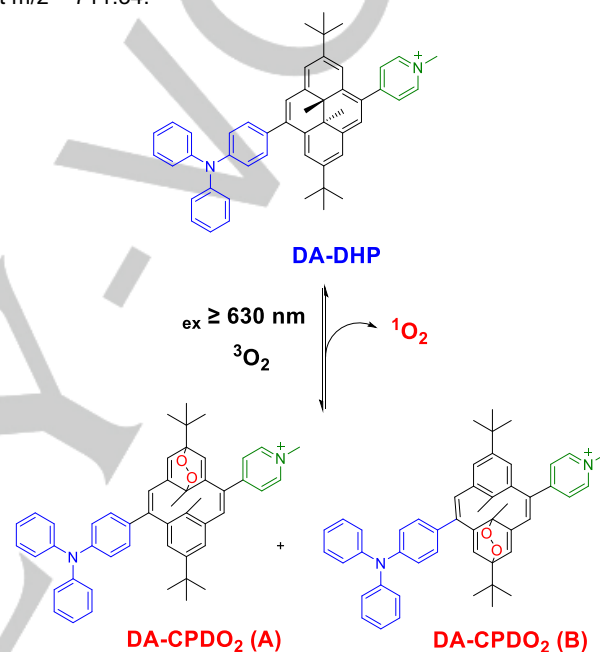
Fluorescence properties

The fluorescence properties of CH_3CN solutions of **DA-DHP** and **DA-CPD** were investigated. **DA-DHP** displays a narrow fluorescence signal at 687 nm upon excitation at 470 nm (see Figure S7), attributed to the emission from the first singlet excited state, with a lifetime of 4.3 ns and a fluorescence quantum yield (Φ^{em}) of $2.6 \cdot 10^{-3}$. These data are close to values found for other **DHP** derivatives bearing pyridinium substituents and the low value of Stokes shift ($+11 \text{ nm} / 0.029 \text{ eV}$) indicates that the **DA-DHP** adopts similar geometries in its ground state and in its lowest excited state. The emission wavelength can be theoretically estimated from the $S_1 \rightarrow S_0$ vertical transition energy computed at **DA-DHP***. The TD-DFT result gives an emission wavelength of 698 nm in acetonitrile, and the computed Stokes shift is 70 nm (0.198 eV), in good agreement with that observed experimentally. When the solution of **DA-DHP** was irradiated by visible light ($\lambda_{\text{ex}} \geq 630 \text{ nm}$) at room temperature, the photo-opening of the central C-C bond was accompanied by a decrease in fluorescence, according to the formation of the non-emissive open-ring isomer when excitation is realized at 470 nm.

Reactivity of DA-DHP with dioxygen

As indicated above, upon suitable functionalization, **DHP** derivatives may exhibit a remarkable reactivity with O_2 .^[16] Indeed, during irradiation under aerobic conditions, they may act as photosensitizers allowing the direct production of singlet oxygen ($^1\text{O}_2$, first excited state of dioxygen) and they may also form endoperoxide derivatives by reaction between the photo-generated open-ring isomers and $^1\text{O}_2$ (*i.e.* $\text{CPD} + ^1\text{O}_2 \rightarrow \text{CPDO}_2$). In order to evaluate the ability of **DA-DHP** to react with O_2 , a CH_3CN solution of this compound was illuminated by red light ($\lambda_{\text{ex}} \geq 630 \text{ nm}$) under aerobic atmosphere (air, 1 atm.). During irradiation, the initial **DA-DHP** was rapidly and completely consumed and the solution became light yellow. Evolution of the solution was followed by UV/vis and ^1H NMR spectroscopies. The final ^1H -NMR spectrum (when no more evolution was observed) obtained upon illumination is given in Figure 1C. Clearly, the two **DA-DHP** and **DA-CPD** isomers were not detected and new sets of signals were obtained at the end of the experiment. Analysis showed that two products were formed with molar proportions equal to 2:1. The starting **DA-DHP** product being unsymmetrical because of the presence of two different substituents, the photogenerated compounds were identified as two endoperoxide

derivatives (named **DA-CPDO**₂, forms **A** and **B**, Scheme 3) in which the position of the peroxide group can be located on the two different benzene rings of the CPD structure. In particular, the two singlets observed at ca. 0 ppm are attributed to proton signals of the internal $-\text{CH}_3$ bound to the peroxide group and constitute a real signature corroborating the presence of two endoperoxide compounds. NMR analysis also shows that the donor part of the compound, *i.e.* the tris-phenylamino group, is not oxidized during the reaction. In addition, it should be noted that the solution containing the two **DA-CPDO**₂ isomers was analyzed by several 1D and 2D NMR techniques, but the major endoperoxide form that was obtained could not be unambiguously attributed. The formation of **DA-CPDO**₂ was also corroborated by mass spectrometry experiments, with a signal corresponding to $[\text{M}+\text{O}_2]$ at $m/z = 711.34$.



Scheme 3. Reversible formation of two endoperoxide isomers (**DA-CPDO**₂, forms **A** and **B**) by illumination of **DA-DHP** with red light under aerobic conditions.

DFT calculations could confirm the existence of the two endoperoxide isomers **A** and **B** of **DA-CPDO**₂ (Figure 6). To investigate the cycloaddition pathways of $^1\text{O}_2$ with CPD, two electrostatic complexes denoted **DA-CPD** $\cdots^1\text{O}_2$ (**A**) and **DA-CPD** $\cdots^1\text{O}_2$ (**B**) were first optimized with $^1\text{O}_2$ approaching CPD on its two different benzene rings. These complexes provide stable structures allowing the two reactants to interact in order to proceed to the endoperoxide formation. According to a previous DFT study of the cycloaddition pathways of $^1\text{O}_2$ with CPD for a bis-pyridinium appended system, the concerted cycloaddition pathway is more favorable than the stepwise mechanism.^[28] This is also the case for the cycloaddition of $^1\text{O}_2$ with benzene.^[29] Thus, we only computed the concerted pathway herein. The results are provided in Figure 6. The two starting complexes are only separated by 0.1 kcal/mol and can be considered degenerate. The concerted transition states are associated with potential energy barriers of 8.6 and 9.5 kcal/mol for **A** and **B** isomers, respectively. The formation of the two corresponding endoperoxides is energetically favorable. They are lying about 12

FULL PAPER

kcal/mol below the reactant **DA-CPD**•••¹O₂ complexes. The two endoperoxides are quasi-isoenergetic with the **A** isomer lower than the **B** one by only 0.5 kcal/mol. The results of these two concerted cycloaddition pathways thus suggest that the formation of the **A** isomer would be favored over the formation of the **B** isomer. One can also note that only mono-endoperoxide forms were obtained and that the formation of the bis-endoperoxide, certainly energetically unfavored, was not observed.

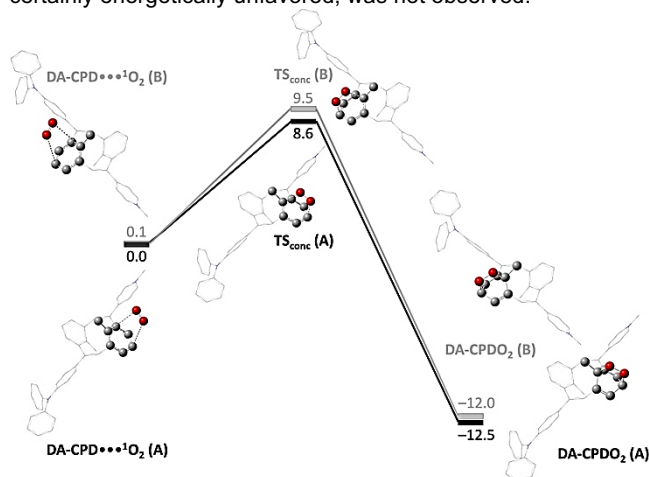
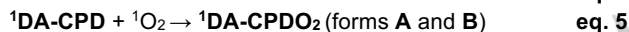
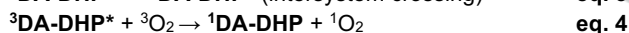


Figure 6. DFT cycloaddition concerted pathways between **DA-CPD** and ¹O₂ forming the two endoperoxides **DA-CPDO₂** (**A**) and (**B**). Energies are given in kcal/mol relative to the lowest electrostatic complex **DA-CPD**•••¹O₂ (**A**). Black and grey lines show the two distinct paths leading to the two endoperoxides **DA-CPDO₂** (**A** and **B**, respectively) via concerted transition states (TS_{conc}). The ¹O₂ molecule and the interacting methylbenzene ring of **DA-CPD** are shown in ball and sticks. Hydrogen atoms are not shown for clarity reasons.

The formation of these two endoperoxide forms is explained by the following simplified mechanism (eq. 1-5):



During illumination, **DA-DHP** which is excited (eq. 1) can then be opened to form **DA-CPD** (eq. 2) and may also act as O₂ sensitizer to generate ¹O₂ (eq. 4) after intersystem crossing to its triplet excited state (eq. 3). **DA-CPD** can then react with ¹O₂ to generate the endoperoxide derivatives **DA-CPDO₂**, forms **A** and **B** (eq. 5). The formation of **DA-CPD** as an intermediate is clearly seen when the reaction is followed by NMR.

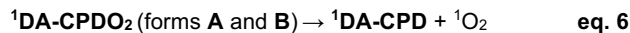
The reaction describes by eq. 5, was demonstrated by an additional NMR experiment: to a solution of freshly prepared **DA-CPD** (obtained by illumination of **DA-DHP** under inert atmosphere), were added 10 mol% of tetraphenylporphyrin (TPP), which is a well-known O₂ photosensitizer.^[30] Upon irradiation of the solution by visible light (λ ≥ 490 nm, where only TPP absorbs), the quantitative formation of **DA-CPDO₂** (forms **A** and **B**) was rapidly observed (see Figure S15). This demonstrates the efficiency of the reaction between the **DA-CPD** isomer and singlet oxygen. Interestingly, the molar proportion of the two generated endoperoxide forms **A** and **B** was 2:1, which is identical to what has been observed previously when **DA-DHP** was illuminated in the presence of air.

The photo-production of singlet oxygen (eq. 4) was then realized by continuous irradiation of **DA-DHP** with visible light under air (1 atm.) in the presence of 15 molar eq. of 2,3-dimethyl-2-butene (90 mM), which is known to react with O₂ to give a hydroperoxide. The reaction was followed by proton NMR and the data show that the hydroperoxide was gradually produced during illumination and the starting alkene was almost consumed (yield: 89%) upon 74 hours of irradiation. It is important to note that the production of endoperoxide from the simple dimethyldihydropyrene has been reported, but it proceeds with low yields and with higher energy of illumination.^[31]

Importantly, the above mechanism is only possible if **DA-DHP** can be populated in its lowest triplet excited state by intersystem crossing (ISC) as shown in eq. (3). Our theoretical calculations of the triplet states along the initial S₁ relaxation pathway (Figure S21) show that the energy gap between S₁ and the triplet states T₂ and T₃ is getting smaller, reaching only 3.5 and 1.8 kcal/mol at the S₁ minimum geometry. The spin-orbit couplings (SOCs) between S₁ and these two triplet states are computed at 1.5 and 2.5 cm⁻¹, respectively, at this geometry. In addition, the minimum energy crossing point between S₁ and T₃ has been located at only 0.05 kcal/mol above the S₁ minimum, making this funnel for S₁→T₃ ISC easily accessible energetically. The SOC values are unchanged within 0.1 cm⁻¹ at this crossing geometry. All these results thus point to a possible S₁→T₃ ISC, reminiscent to what was found for a bispyridinium-appended DHP for which an S₁→T₂ ISC was proposed.^[28]

Thermal releasing of ¹O₂ from **DA-CPDO₂**

It is recognized that aromatic endoperoxides can act as chemical sources of ¹O₂ following a clean decomposition reaction upon heating.^[32-34] The thermal stability of **DA-CPDO₂** was investigated using UV/vis absorption spectroscopy. Upon heating at 37°C, the yellowish solution of **DA-CPDO₂** (forms **A** and **B**) in CH₃CN gradually turned red and the UV/vis spectrum of the parent closed state **DA-DHP** was fully recovered within a few hours, indicating the cleavage of the peroxidic unit and thus, the complete reversibility of O₂ binding. This result was corroborated by ¹H NMR spectroscopy that shows that **DA-CPDO₂** cycloreverts to **DA-CPD** upon heating, which then thermally isomerizes to yield the initial **DA-DHP**, as described by equations 6 and 7 (Figure S16, S17):



The amount of singlet oxygen thermally released was quantified using NMR trapping experiments. A freshly prepared solution of **DA-CPDO₂** (3.9 mM) was left at 37°C in the dark in the presence of 2,3-dimethyl-2-butene (117 mM). Upon 48 hours, the starting **DA-DHP** was fully recovered and the yield of produced hydroperoxide was 60 ± 10 % (measured by integration of the ¹H-NMR signals). Considering that the reaction between ¹O₂ and 2,3-dimethyl-2-butene is usually not quantitative due to the short lifetime of singlet dioxygen, the amount of ¹O₂ delivered by **DA-CPDO₂** is certainly underestimated.

Conclusion

We have reported the synthesis and characterization of a photochromic system (**DA-DHP**) based on the dimethyldihydropyrene (**DHP**) unit. Using consecutive Suzuki-reaction couplings, both donor and acceptor units have been incorporated onto the **DHP** core. Spectroscopic and electrochemical characterizations associated to theoretical calculations showed that this functionalization allows a modification of the redox properties and a significant red-shift of the absorption spectrum of the photochromic **DHP** center. As a consequence, the photoisomerization of **DA-DHP** to its corresponding cyclophanediene form (**DA-CPD**) proceeds by illumination at low energy with very high quantum yield ($\Phi_{c-o} = 13.3\%$ at $\lambda_{ex} = 660$ nm for **DA-DHP** vs. $\Phi_{c-o} = 0.08\%$ at $\lambda_{ex} = 470$ nm for the non-functionalized **DHP**). In addition, when illuminated with red light under aerobic conditions at room temperature, **DA-DHP** was shown to quantitatively trap molecular oxygen and two endoperoxide isomers (**DA-CPDO₂**, forms **A** and **B**) are produced. This reaction is reversible: **DA-DHP** and singlet oxygen can then be produced by heating a solution of **DA-CPDO₂**. The efficient photochromic behavior and the particular reactivity towards dioxygen of the **DA-DHP** system can be explored for several domains such as photochromic materials and devices, photodynamic therapy or (photo-)oxidation reactions.

Experimental Section

Materials and instrumentation. All solvents were purchased and used as received except THF that was distilled over sodium/ benzophenone under argon. Water was purified by reverse osmometry with an Elgastat purification system (5 M Ω .cm). Organic and inorganic reagents used in the procedures described below were purchased on Aldrich, Acros, Fluorochem or TCI Europe and used without further purification. All evaporations were carried out under reduced pressure with a rotatory evaporator, and all organic extract were washed with water and dried with MgSO₄. Silica gel used for column chromatography refers to Merck silica gel, 40-63 μ m. Melting points were measured thanks to capillary tubes on a Büchi B-545 device. Infrared spectra (IR) were recorded on a Perkin Elmer Spectrum Two Fourier transform infrared spectrometer using ATR (Attenuated Total Reflexion) modes. ¹H NMR and ¹³C NMR spectra were recorded on a Bruker Avanced 500 or 400 MHz spectrometer in CD₂Cl₂ or CD₃CN. Chemical shifts are calibrated to residual solvent peaks. Coupling constant values (J) are given in hertz and chemical shifts (δ) in ppm. High-resolution mass spectrometry analyses were conducted using the HRMS, Bruker maXis mass spectrometer and were performed in positive Electrospray Ionisation (ESI⁺) at the DCM mass facility.

Data for single crystal X-Ray diffraction were collected at room temperature on a Bruker AXS Enraf-Nonius Kappa CCD diffractometer using the Cu-K α graphite monochromated radiation. Intensity data were collected for Lorentz and polarization effects with EVAL 14 and for absorption using SADABS. Structures solutions and refinements were performed with the SHELX softwares implemented by Olex2. All non-hydrogen were refined by full matrix least-squares with anisotropic thermal parameters. Hydrogen atoms were introduced at calculated positions as riding atoms. Crystallographic structures were drawn with the Mercury 2020.3.0 software. A summary of the data collection and structure refinements is provided in the supplementary information. CCDC 2093111 (**D-DHP**) contains the supplementary crystallographic data for this paper. These data can be obtained free of charge from The Cambridge Crystallographic Data Centre via www.ccdc.cam.ac.uk/data_request/cif.

Electrochemical measurements (cyclic voltammetry, CV) were conducted under an argon atmosphere with a standard one-compartment, three-electrode electrochemical cell using a CH-Instrument 660B potentiostat.

Anhydrous CH₃CN or CH₂Cl₂ were used as solvents and tetra-*n*-butylammonium hexafluorophosphate (TBAPF₆, 0.1M) was used as supporting electrolyte. CH-Instrument vitreous carbon (3 mm in diameter) working electrodes were used for CV experiments. Electrodes were polished with 1 μ m diamond paste (Mecaprex Presi) prior to each recording. Counter-electrode was a platinum wire immersed directly in the solution. A CH-Instrument AgNO₃/Ag (10⁻² M + tetra-*n*-butylammonium perchlorate 10⁻¹ M in CH₃CN) electrode was used as a reference electrode and the potential of the regular ferrocenium / ferrocene (Fc⁺/Fc) redox couple in acetonitrile is 0.07 V under our experimental conditions. Cyclic voltammetry (CV) curves were recorded at a scan rate of 0.1 V s⁻¹. An automatic ohmic drop compensation procedure was systematically implemented prior to recording CV data.

Spectroscopy, irradiation procedures and quantum yields measurements. UV/vis absorption spectra were recorded using a Varian Cary 60 spectrophotometer with temperature controller. The measurements over the spectral range from 250 to 800 nm were carried out in Hellma quartz cells (QS) having an optical path length of 1 cm. Emission spectra were recorded in CH₃CN at room temperature on a Horiba Fluoromax fluorescence spectrophotometer. Samples were placed in 1 cm optical path length quartz cells. Luminescence lifetimes measurements were performed using a 400 nm irradiation wavelength obtained by the second harmonic of a titanium: sapphire laser (picosecond Tsunami laser spectra physics 3950-M1BB and 39868-03 pulse picker doubler) at 800 kHz repetition rate. Fluotime 200 from AMS technologies was used for the decay acquisition. It is composed of a GaAs microchannel plate photo-multiplier tube (Hamamatsu model R3809U-50) followed by a time-correlated single-photon counting system from Picoquant (PicoHarp300). Luminescence decays were analyzed with Fluofit software available from Picoquant. Emission quantum yields Φ^{Em} were determined at room temperature in CH₃CN solutions ($\lambda_{ex} \approx 480$ nm). The [Ru(bpy)₃]²⁺ complex in aqueous solution was used as quantum yield standard ($\Phi^{Em} = 0.028$) according to the following equation:

$$\Phi_s^{Em} = \Phi_{Ru(bpy)_3}^{Em} \times \frac{Abs_{Ru(bpy)_3}}{Abs_s} \times \frac{I_s}{I_{Ru(bpy)_3}} \times \frac{n_{CH_3CN}^2}{n_{H_2O}^2}$$

Where s and Ru(bpy)₃ denote the sample and the standard respectively. I is the integrated emission intensity, Abs the absorption at the excitation wavelength and n the refractive index of the solvent.

All the irradiation experiments were performed in solution, using different cells (classical UV/vis, quartz cells, NMR tubes). The visible irradiations were carried out with a Xe-Hg lamp (500W) equipped with cut-off filters or with Thorlabs mounted LEDs of specific wavelengths combined with an adjustable Thorlab collimation adapter. The samples were kept at 4°C during irradiation in order to limit the thermal back reaction. The open to closed isomerization was investigated by irradiation at 254 nm or 366 nm using a hand-held chromatography lamp (7W). Samples were placed at 15 cm from the visible light Xe-Hg lamp and 4 cm from the UV lamp or LEDs. For the experiments under anaerobic conditions, all the samples were prepared in a Jacomex glove box with carefully degassed deuterated and non-deuterated solvent.

The conversion between the closed (DHPs) and open (CPDs) isomers was investigated with UV/vis and NMR experiments at 4°C. It was considered that the photo-stationary state was reached when no evolution was observed in three consecutive intermediate spectra or after a long period of irradiation. The ratio between DHP and CPD forms was determined by ¹H NMR from the relative integration of their characteristic resonance peaks of the internal methyl groups. This ratio was also determined with UV/vis spectroscopy by comparing the intensity of the DHP absorption band (visible region) before and after irradiation. Quantum yields for the photo-induced ring-opening process (DHPs→CPDs, Φ_{c-o}) were determined by illumination of solutions of DHP derivatives at 4°C using LEDs at specific wavelengths. The light power was measured with a Newport (818-SL) photodetector and the photoconversion was followed by

UV/vis absorption spectroscopy. Illuminations and absorption measurements were performed at wavelengths for which only the closed-ring isomers absorb. Data were extracted by fitting of the experimental curves using the kinetic model reported by Maafi and Brown.^[21,22]

Computations. Density functional theory (DFT) and its time-dependent version (TD-DFT) were used to perform calculations on the ground and excited states, respectively, of the four studied DHPs shown in Chart 1 (i.e., **DA-DHP**, **A-DHP**, **D-DHP** and **DHP**). Ground-state geometry optimizations were carried out with the hybrid B3LYP functional,^[35] while excited states were computed and optimized with the long-range corrected hybrid ω B97X-D functional^[36] within linear-response TD-DFT. Pople's 6-311G(d,p) basis set was used throughout.^[37] All calculations were performed with the corresponding solvent used in the experiment (i.e., cyclohexane for **D-DHP** and **DHP**, and acetonitrile for **DA-DHP** and **A-DHP**) within the integral equation formalism polarizable continuum model (IEFPCM).^[38] Vertical absorption transition energies were computed using linear-response non-equilibrium solvation. Note that within the crude vertical approximation, deviations of about 0.25 eV are rather common for valence excited states of organic molecules computed with TD-DFT.^[39] Calculation of the emission wavelength was carried out using the more accurate external iteration state-specific non-equilibrium approach.^[40] Natural transition orbitals (NTOs)^[41] for relevant electronic transitions were generated in order to compare the nature of the excited states involved between the various studied DHPs.

Transition state for the thermal **DA-CPD** to **DA-DHP** conversion was located using broken-symmetry DFT due to the biradical (open-shell singlet) nature of this species. To account for the spin contamination, spin-projected energies were computed with the approximate spin-correction procedure proposed by Yamaguchi and coworkers.^{[42], [43]} The associated activation energy was estimated from the spin-projected energy at the transition state taking also into account thermochemical corrections. The cycloaddition of **DA-CPD** with $^1\text{O}_2$ was also investigated with broken-symmetry DFT. For this mechanism, the two *tert*-butyl groups were replaced by hydrogen atoms to reduce the computational cost. All DFT and TD-DFT calculations were performed with Gaussian 16.^[44]

The photoisomerization pathway of **DA-DHP** was computed with spin-flip TD-DFT (SF-TD-DFT)^[45] in the gas phase. This quantum chemical method allows the correct physical description of S_0/S_1 conical intersection, unlike TD-DFT.^[46–49] It uses a triplet reference state to generate the singlet ground state and electronic excited states applying one-electron spin-flip excitations. Thus, ground and excited states are described on an equal footing, in contrast to TD-DFT. SF-TD-DFT calculations were performed within the Tamm-Dancoff approximation using a spin-restricted triplet reference. For these calculations, the recommended half-and-half BHHLYP functional^[50] was used and the *tert*-butyl groups were also replaced by hydrogen atoms. GAMESS^[51] was used to carry out the SF-TD-DFT calculations. Note that because analytic hessian is not implemented at the SF-TD-DFT in GAMESS, the excited-state transition state was optimized with TD-DFT to evaluate the excited-state barrier on S_1 along the **DA-DHP** to **DA-CPD** photoisomerization.

Triplet excited states were also computed along the S_1 initial photoisomerization pathway at the TD-DFT level using ω B97X-D/6-311G(d,p). The Tamm-Dancoff approximation was used for a more reliable description of the singlet/triplet energy gaps.^[52] Calculations of spin-orbit couplings and optimization of the minimum energy crossing point between S_1 and T_3 were performed using Q-Chem 5.4.^[53]

All the optimized Cartesian coordinates are collected in Supporting Information.

Synthetic procedures

2,7-di-*tert*-butyl-*trans*-10b,10c-dimethyl-10b,10c-dihydropyrene, 4-bromo-2,7-di-*tert*-butyl-*trans*-10b,10c-dimethyl-10b,10c-dihydropyrene and 4,9-

dibromo-2,7-di-*tert*-butyl-*trans*-10b,10c-dimethyl-10b,10c-dihydropyrene, 4-(2,7-di-*tert*-butyl-*trans*-10b,10c-dimethyl-10b,10c-dihydropyren-4-yl)-1-methylpyridin-1-ium hexafluorophosphate (**A-DHP**) were synthesized following reported procedure.^[16]

4-(2,7-di-*tert*-butyl-*trans*-10b,10c-dimethyl-10b,10c-dihydropyren-4-yl)-*N,N*-diphenylaniline (D-DHP): A round bottom flask was filled with 4-bromo-2,7-di-*tert*-butyl-*trans*-10b,10c-dimethyl-10b,10c-dihydropyrene (50 mg, 0.10 mmol), 4-(diphenylamino)phenylboronic acid (38 mg, 0.13 mmol, 1.3 equiv.) and freshly distilled THF (6 mL). A degassed aqueous solution (3 mL) of potassium carbonate (65 mg, 0.48 mmol, 4.8 equiv.) and tetrakis(triphenylphosphine) palladium (0) (21 mg, 0.022 mmol) were added into the flask and the resulting mixture was heated to reflux under stirring for 48 h. After cooling down the mixture to room temperature, the solvent was evaporated under reduced pressure until dryness. The solid residue was dissolved in CH_2Cl_2 (50 mL) and the solution was filtered over celite. The resulting solution was washed with water (3 x 50 mL), brine (50 mL), dried over anhydrous MgSO_4 and evaporated under reduced pressure. The crude product was purified by column chromatography on silica gel using cyclohexane as eluent. The desired product was obtained as a dark green solid (25 mg, 0.042 mmol) with 42% yield. m.p: 208–210°C. IR: 3034, 2959, 2953, 2924, 2903, 2865, 1589, 1486, 1270, 882, 751, 696, 666, 624, 508 cm^{-1} . ^1H RMN (400 MHz, CD_2Cl_2) δ : 8.78 (s, 1H, H_{ar}), 8.57 (s, 2H, H_{ar}), 8.56 (s, 1H, H_{ar}), 8.53 (s, 1H, H_{ar}), 8.46 (s, 2H, H_{ar}), 7.80–7.72 (m, 2H, H_{ar}), 7.37–7.30 (m, 6H, H_{ar}), 7.29–7.21 (m, 4H, H_{ar}), 1.71 (s, 9H, H_{tBu}), 1.64 (s, 9H, H_{tBu}), -3.84 (s, 3H, H_{Me}), -3.87 (s, 3H, H_{Me}). HRMS (ESI) m/z : Calc. for $\text{C}_{44}\text{H}_{45}\text{N}$ 587.3532. Found. 587.3536. UV/vis (λ_{max} [nm] ϵ [$\text{M}^{-1}\text{cm}^{-1}$]): 652 (1000), 484 (8000), 470 (8000), 395 (45000), 348 (48000). (^{13}C NMR signal could not be collected due to the low solubility of the compound, but a X-ray structure was obtained, see S.I.)

4-(9-dibromo-2,7-di-*tert*-butyl-*trans*-10b,10c-dimethyl-10b,10c-dihydropyren-4-yl)pyridine (2): A round bottom flask was filled under an argon atmosphere with compound (1) (50 mg, 0.1 mmol), 4-pyridinylboronic acid (13 mg, 0.1 mmol, 1 equiv.) and freshly distilled THF (6 mL). A degassed aqueous solution (3 mL) of potassium carbonate (67 mg, 0.48 mmol, 4.8 equiv.) and tetrakis(triphenylphosphine) palladium (0) (18 mg, 0.016 mmol) were added into the flask and the resulting mixture was heated to reflux under stirring for 72 h. After cooling down the mixture to room temperature, the solvent was evaporated under reduced pressure until dryness. The solid residue was dissolved in CH_2Cl_2 (50 mL) and the solution is filtered over celite. The resulting solution was washed with water (3 x 50 mL), brine (50 mL), dried over anhydrous MgSO_4 and evaporated under reduced pressure. The crude product was purified by column chromatography over silica gel using cyclohexane:ethyl acetate gradient (1:0 to 93:7) (v:v). Compound (2) was obtained as a dark green solid (27 mg, 0.054 mmol) with 54% yield. m.p: 221–223°C. IR: 3059, 3019, 2960, 2952, 2962, 2904, 2865, 1592, 1238, 904, 897, 800, 671, 533 cm^{-1} . ^1H RMN (400 MHz, CDCl_3) δ : 8.88–8.83 (m, 3H, H_{ar}), 8.69 (d, 1H, H_{ar}), 8.62 (s, 2H, H_{ar}), 8.52 (s, 1H, H_{ar}), 8.48 (s, 1H, H_{ar}), 7.80 (d, $J = 8$ Hz, 2H, H_{ar}), 1.75–1.72 (m, 9H, H_{tBu}), 1.61 (s, 9H, H_{tBu}), -3.69 (s, 3H, H_{Me}), -3.73 (s, 3H, H_{Me}). ^{13}C RMN (100 MHz, CD_3CN) δ : 149.5, 147.9, 137.8, 132.5, 132.4, 128.7, 128.6, 126.8, 126.1, 125.1, 123.0, 122.1, 121.2, 32.00, 31.8, 14.9, 14.6. HRMS (ESI) m/z : Calc. for $\text{C}_{31}\text{H}_{35}\text{Br}^+$ 500.1953. Found. 500.1957.

4-(2,7-di-*tert*-butyl-*trans*-10b,10c-dimethyl-9-(pyridine-4-yl)-10b,10c-dihydropyren-4-yl)-*N,N*-diphenylaniline (3): A round bottom flask was filled under an argon atmosphere with the compound (2) (27 mg, 0.054 mmol), 4-(diphenylamino)phenylboronic acid (20.2 mg, 0.07 mmol, 1.3 equiv.) and freshly distilled THF (6 mL). A degassed aqueous solution (2 mL) of potassium carbonate (36 mg, 0.26 mmol, 4.8 equiv.) and tetrakis(triphenylphosphine) palladium (0) (12 mg, 0.010 mmol) were added into the flask and the resulting mixture was heated to reflux under stirring for 72 h. After cooling down the mixture to room temperature, the solvent was evaporated under reduced pressure until dryness. The solid residue was dissolved in CH_2Cl_2 (50 mL) and the solution is filtered over celite. The resulting solution was washed with water (3 x 50 mL), brine (50 mL), dried over anhydrous MgSO_4 and evaporated under reduced pressure. The crude

product was purified by column chromatography over silica gel using cyclohexane:ethyl acetate gradient (1:0 to 95:5) (v:v). The desired product (**3**) was obtained as an orange solid (28 mg, 0.042 mmol) with 78% yield. m.p.: 93–96°C. IR: 3057, 3029, 2957, 2924, 2867, 1590, 1491, 1266, 893, 832, 750, 692, 667 cm⁻¹. ¹H NMR (400 MHz, CD₂Cl₂) δ: 8.81 (m, 3H, H_{ar}), 8.64 (s, 1H, H_{ar}), 8.60 (d, J = 8 Hz, 2H, H_{ar}), 8.54 (s, 1H, H_{ar}), 8.47 (s, 1H, H_{ar}), 7.77 (dd, J₁ = 18 Hz, J₂ = 7 Hz, 4H, H_{ar}), 7.34 (m, 6H, H_{ar}), 7.26 (d, J = 8 Hz, 4H, H_{ar}), 7.09 (t, J = 7 Hz, 2H, H_{ar}), 1.63 (s, 9H, H_{IBu}), 1.61 (s, 9H, H_{IBu}), -3.68 (s, 3H, H_{Me}), -3.69 (s, 3H, H_{Me}). ¹³C NMR (400 MHz, CD₂Cl₂) δ: 151.19, 150.00, 148.49, 147.52, 147.47, 146.87, 137.78, 137.18, 137.16, 135.73, 133.93, 132.33, 131.86, 129.91, 126.57, 126.53, 125.82, 125.03, 124.83, 124.07, 123.52, 122.52, 121.93, 121.33, 119.47, 36.64, 36.59, 32.11, 32.08, 30.91, 30.75, 15.19, 15.18. HRMS (ESI) *m/z*: Calc. for C₄₉H₄₉N₂⁺ 665.3897. Found. 665.3887.

4-(2,7-di-*tert*-butyl-9-(4-(diphenylamino)phenyl)-10b,10c-dimethyl-10b,10c-dihydropyrene-4-yl)-1-methylpyridin-1-ium

hexafluorophate (DA-DHP): A solution of the compound (**3**) (28 mg, 0.042 mmol) in CH₂Cl₂ (5 mL) is degassed. Methyl iodide (1 mL) was added to the previous solution and the resulting mixture was allowed to stir for 4 h under inert atmosphere. After the required time, the solvent was evaporated under reduced pressure and the residue was then dissolved in MeOH (1 mL). The product was subjected to an anion exchange using a saturated aqueous solution of KPF₆ (2 mL). The solid was filtered under vacuum and washed several times with water and diethyl ether. The solid was then dried under reduced pressure to give the targeted product as a red powder (32 mg, 0.039) in 93% yield. If needed, the compound can be further purified either by column chromatography over silica gel using a mixture of Acetonitrile:MeOH:H₂O:NaBr (4:1:1:1) (v:v:v:v) followed by an anion exchange using a saturated aqueous solution of KPF₆ (2 mL) in methanol (1 mL) or by a recrystallization in methanol. m.p.: 241–243°C. IR: 3032, 2959, 2923, 2906, 2867, 1634, 1588, 1503, 1489, 831, 751, 695, 556 cm⁻¹. ¹H NMR (500 MHz, CD₃CN) δ: 8.84 (s, 1H, H_{ar}), 8.78 (s, 1H, H_{ar}), 8.77 (s, 1H, H_{ar}), 8.74 (d, J = 7 Hz, 2H, H_{ar}), 8.70 (s, 1H, H_{ar}), 8.62 (s, 1H, H_{ar}), 8.63 (s, 1H, H_{ar}), 8.44 (d, J = 7 Hz, 2H, H_{ar}), 7.76 (d, J = 9 Hz, 2H, H_{ar}), 7.38 (m, 4H, H_{ar}), 7.32 (d, J = 9 Hz, 2H, H_{ar}), 7.23 (dd, J₁ = 8 Hz, J₂ = 1 Hz, 4H, H_{ar}), 7.13 (tt, J₁ = 8 Hz, J₂ = 1 Hz, 2H, H_{ar}), 4.40 (s, 3H, H_{NMe}), 1.65 (s, 9H, H_{IBu}), 1.62 (s, 9H, H_{IBu}), -3.65 (s, 3H, H_{Me}), -3.67 (s, 3H, H_{Me}). ¹³C NMR (125 MHz, CD₃CN) δ: 159.73, 150.48, 148.78, 148.40, 148.11, 145.47, 139.70, 137.80, 137.47, 136.69, 134.81, 134.59, 132.80, 130.55, 130.07, 127.88, 126.56, 125.56, 125.52, 124.75, 124.40, 124.38, 124.11, 123.22, 123.10, 48.44, 37.13, 36.83, 31.90, 31.81, 31.67, 30.94, 15.48, 15.44. HRMS (ESI) *m/z*: DA-DHP: Calc. for C₅₀H₅₁N₂⁺ 679.4047. Found. 679.4042. ESI-MS (ESI) *m/z*: DA-CPD: Calc. for C₅₀H₅₁N₂⁺ 679.41. Found. 679.35. ESI-MS (ESI) *m/z*: DA-CPDO₂: Calc. for C₅₀H₅₁N₂O₂⁺ 711.39. Found. 711.34. UV/vis (λ_{max} [nm] ε [M⁻¹.cm⁻¹]): 676 (2000), 535 (6000), 422 (18000), 341 (27000), 304 (22000). φ^{Em} = 2.6 · 10⁻³. τ = 4.3 ns.

Acknowledgements

This work was supported by the French Agence National de la Recherche (Grant ANR-18-CE29-0012 PHOTOCROMICS). The NanoBio ICMG (UAR 2607) is acknowledged for providing facilities for mass spectrometry analyses (A. Durand, L. Fort, R. Gueret) as well as the DCM (Département de Chimie Moléculaire, Plateau Technique de Synthèse) for the synthesis of the DHP precursors (Martine Fayolle, Mathieu Curtil, Pierre-Yves Chavant). This work was granted access to the HPC resources of CALMIP supercomputing center under the allocation 2021-[12158].

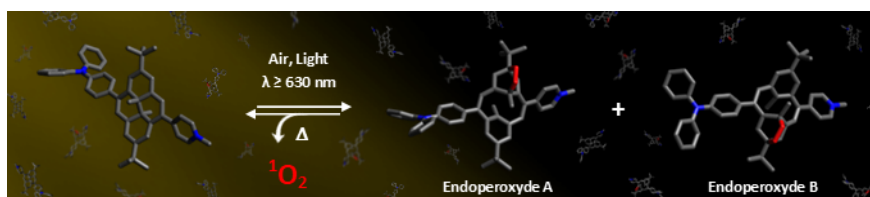
Keywords: photochromism • dimethyldihydropyrene • singlet oxygen • endoperoxide • spin-flip time-dependent density functional theory

[1] G. Berkovic, V. Krongauz, V. Weiss, *Chem. Rev.* **2000**, *100*, 1741–1754.

- [2] S. Helmy, S. Oh, F. A. Leibfarth, C. J. Hawker, J. Read de Alaniz, *J. Org. Chem.* **2014**, *79*, 11316–11329.
- [3] S. Helmy, F. A. Leibfarth, S. Oh, J. E. Poelma, C. J. Hawker, J. Read de Alaniz, *J. Am. Chem. Soc.* **2014**, *136*, 8169–8172.
- [4] A. C. V. Baizani, M. Venturi, *Molecular Devices and Machines*, Wiley-VCH, Weinheim, **2008**.
- [5] B. L. Feringa, W. R. Browne, Editors, *Molecular Switches, Volume 2: Second, Completely Revised and Enlarged Edition*, Wiley-VCH Verlag GmbH & Co. KGaA, **2011**.
- [6] W. A. Velema, W. Szymanski, B. L. Feringa, *J. Am. Chem. Soc.* **2014**, *136*, 2178–2191.
- [7] W. Szymański, J. M. Beierle, H. A. V. Kistemaker, W. A. Velema, B. L. Feringa, *Chem. Rev.* **2013**, *113*, 6114–6178.
- [8] L. Hou, X. Zhang, T. C. Pijper, W. R. Browne, B. L. Feringa, *J. Am. Chem. Soc.* **2014**, *136*, 910–913.
- [9] J. Ji, X. Li, T. Wu, F. Feng, *Chem. Sci.* **2018**, *9*, 5816–5821.
- [10] M. Jacquet, L. M. Uriarte, F. Lafolet, M. Boggio-Pasqua, M. Sliwa, F. Loiseau, E. Saint-Aman, S. Cobo, G. Royal, *J. Phys. Chem. Lett.* **2020**, *11*, 2682–2688.
- [11] R. H. Mitchell, *Eur. J. Org. Chem.* **1999**, *1999*, 2695–2703.
- [12] C. Bohne, R. H. Mitchell, *J. Photochem. Photobiol. C Photochem. Rev.* **2011**, *12*, 126–137.
- [13] K. Klaue, W. Han, P. Liesfeld, F. Berger, Y. Garmshausen, S. Hecht, *J. Am. Chem. Soc.* **2020**, *142*, 11857–11864.
- [14] K. Klaue, Y. Garmshausen, S. Hecht, *Angew. Chem. Int. Ed.* **2018**, *57*, 1414–1417.
- [15] E. Lognon, M.-C. Heitz, A. Bakkar, S. Cobo, F. Loiseau, E. Saint-Aman, G. Royal, M. Boggio-Pasqua, *ChemPhysChem* **2020**, *21*, 1571–1577.
- [16] D. Roldan, S. Cobo, F. Lafolet, N. Vilà, C. Bochet, C. Bucher, E. Saint-Aman, M. Boggio-Pasqua, M. Garavelli, G. Royal, *Chem. - Eur. J.* **2015**, *21*, 455–467.
- [17] S. Cobo, F. Lafolet, E. Saint-Aman, C. Philouze, C. Bucher, S. Silvi, A. Credi, G. Royal, *Chem. Commun.* **2015**, *51*, 13886–13889.
- [18] A. Bakkar, S. Cobo, F. Lafolet, E. Saint-Aman, G. Royal, *J. Mater. Chem. C* **2015**, *3*, 12014–12017.
- [19] M. A. L. Sheepwash, R. H. Mitchell, C. Bohne, *J. Am. Chem. Soc.* **2002**, *124*, 4693–4700.
- [20] R. Sarkar, M.-C. Heitz, G. Royal, Martial. Boggio-Pasqua, *J. Phys. Chem. A* **2020**, *124*, 1567–1579.
- [21] M. Maafi, R. G. Brown, *J. Photochem. Photobiol. Chem.* **2007**, *187*, 319–324.
- [22] M. Maafi, R. G. Brown, *Photochem. Photobiol. Sci.* **2008**, *7*, 1360–1372.
- [23] B. G. Levine, C. Ko, J. Quenneville, T. J. Martinez, *Mol. Phys.* **2006**, *104*, 1039–1051.
- [24] N. Minezawa, M. S. Gordon, *J. Phys. Chem. A* **2009**, *113*, 12749–12753.
- [25] A. Nikiforov, J. A. Gamez, W. Thiel, M. Huix-Rotllant, M. Filatov, *J. Chem. Phys.* **2014**, *141*, 124122.
- [26] M. Winslow, W. B. Cross, D. Robinson, *J. Chem. Theory Comput.* **2020**, *16*, 3253–3263.
- [27] R. H. Mitchell, T. R. Ward, Y. Chen, Y. Wang, S. A. Weerawarna, P. W. Dibble, M. J. Marsella, A. Almutairi, Z.-Q. Wang, *J. Am. Chem. Soc.* **2003**, *125*, 2974–2988.
- [28] M. Boggio-Pasqua, M. López Vidal, M. Garavelli, *J. Photochem. Photobiol. Chem.* **2017**, *333*, 156–164.
- [29] M. Boggio-Pasqua, J.-L. Heully, *Theor. Chem. Acc.* **2015**, *135*, 9.
- [30] J. Kou, D. Dou, L. Yang, *Oncotarget* **2017**, *8*, 81591–81603.
- [31] H. Cerfontain, A. Koeberg-Telder, B. H. Bakker, R. H. Mitchell, M. Tashiro, *Liebigs AnnRecl* **1997**, *873*–878.
- [32] W. Fudickar, T. Linker, *Angew. Chem. Int. Ed.* **2018**, *57*, 12971–12975.
- [33] S. Callaghan, M. O. Senge, *Photochem. Photobiol. Sci.* **2018**, *17*, 1490–1514.
- [34] M. Matsumoto, M. Yamada, N. Watanabe, *Chem. Commun.* **2005**, 483–485.
- [35] A. D. Becke, *J. Chem. Phys.* **1993**, *98*, 5648–5652.
- [36] J.-D. Chai, M. Head-Gordon, *Phys. Chem. Chem. Phys.* **2008**, *10*, 6615.
- [37] R. Krishnan, J. S. Binkley, R. Seeger, J. A. Pople, *J. Chem. Phys.* **1980**, *72*, 650–654.
- [38] J. Tomasi, B. Mennucci, R. Cammi, *Chem. Rev.* **2005**, *105*, 2999–3094.
- [39] A. D. Laurent, D. Jacquemin, *Int. J. Quantum Chem.* **2013**, *113*, 2019–2039.
- [40] R. Improta, G. Scalmani, M. J. Frisch, V. Barone, *J. Chem. Phys.* **2007**, *127*, 074504.
- [41] R. L. Martin, *J. Chem. Phys.* **2003**, *118*, 4775–4777.
- [42] K. Yamaguchi, F. Jensen, A. Dorigo, K. N. Houk, *Chem. Phys. Lett.* **1988**, *149*, 537–542.
- [43] S. Yamanaka, T. Kawakami, H. Nagao, K. Yamaguchi, *Chem. Phys. Lett.* **1994**, *231*, 25–33.
- [44] M. J. Frisch, G. W. Trucks, H. B. Schlegel, G. E. Scuseria, M. A. Robb, J. R. Cheeseman, G. Scalmani, V. Barone, G. A. Petersson, H. Nakatsuji, X. Li, M. Caricato, A. V. Marenich, J. Bloino, B. G. Janesko, R. Gomperts, B. Mennucci, H. P. Hratchian, J. V. Ortiz, A. F. Izmaylov, J. L. Sonnenberg, D. Williams-Young, F. Ding, F. Lipparini, F. Egidi, J. Goings, B. Peng, A. Petrone, T. Henderson, D. Ranasinghe, V. G. Zakrzewski, J. Gao, N. Rega, G. Zheng, W. Liang, M. Hada, M. Ehara, K. Toyota, R. Fukuda, J. Hasegawa, M. Ishida, T. Nakajima, Y. Honda, O. Kitao, H. Nakai, T. Vreven, K. Throssell, J. A. Montgomery Jr., J. E.

- Peralta, F. Oglaro, M. J. Bearpark, J. J. Heyd, E. N. Brothers, K. N. Kudin, V. N. Staroverov, T. A. Keith, R. Kobayashi, J. Normand, K. Raghavachari, A. P. Rendell, J. C. Burant, S. S. Iyengar, J. Tomasi, M. Cossi, J. M. Millam, M. Klene, C. Adamo, R. Cammi, J. W. Ochterski, R. L. Martin, K. Morokuma, O. Farkas, J. B. Foresman, D. J. Fox, *Gaussian 16 Rev. B.01*, **2016**.
- [45] Y. Shao, M. Head-Gordon, A. I. Krylov, *J. Chem. Phys.* **2003**, *118*, 4807–4818.
- [46] B. G. Levine, C. Ko, J. Quenneville, T. J. Martinez, *Mol. Phys.* **2006**, *104*, 1039–1051.
- [47] N. Minezawa, M. S. Gordon, *J. Phys. Chem. A* **2009**, *113*, 12749–12753.
- [48] A. Nikiforov, J. A. Gamez, W. Thiel, M. Huix-Rotllant, M. Filatov, *J. Chem. Phys.* **2014**, *141*, 124122.
- [49] M. Winslow, W. B. Cross, D. Robinson, *J. Chem. Theory Comput.* **2020**, *16*, 3253–3263.
- [50] A. D. Becke, *J. Chem. Phys.* **1993**, *98*, 1372–1377.
- [51] M. W. Schmidt, K. K. Baldridge, J. A. Boatz, S. T. Elbert, M. S. Gordon, J. H. Jensen, S. Koseki, N. Matsunaga, K. A. Nguyen, S. Su, T. L. Windus, M. Dupuis, J. A. Montgomery, *J. Comput. Chem.* **1993**, *14*, 1347–1363.
- [52] M. J. G. Peach, M. J. Williamson, D. J. Tozer, *J. Chem. Theory Comput.* **2011**, *7*, 3578–3585.
- [53] Y. Shao, Z. Gan, E. Epifanovsky, A. T. B. Gilbert, M. Wormit, J. Kussmann, A. W. Lange, A. Behn, J. Deng, X. Feng, D. Ghosh, M. Goldey, P. R. Horn, L. D. Jacobson, I. Kaliman, R. Z. Khaliullin, T. Kuš, A. Landau, J. Liu, E. I. Proynov, Y. M. Rhee, R. M. Richard, M. A. Rohrdanz, R. P. Steele, E. J. Sundstrom, H. L. Woodcock, P. M. Zimmerman, D. Zuev, B. Albrecht, E. Alguire, B. Austin, G. J. O. Beran, Y. A. Bernard, E. Berquist, K. Brandhorst, K. B. Bravaya, S. T. Brown, D. Casanova, C.-M. Chang, Y. Chen, S. H. Chien, K. D. Closser, D. L. Crittenden, M. Diedenhofen, R. A. DiStasio, H. Do, A. D. Dutoi, R. G. Edgar, S. Fatehi, L. Fusti-Molnar, A. Ghysels, A. Golubeva-Zadorozhnaya, J. Gomes, M. W. D. Hanson-Heine, P. H. P. Harbach, A. W. Hauser, E. G. Hohenstein, Z. C. Holden, T.-C. Jagau, H. Ji, B. Kaduk, K. Khistyayev, J. Kim, J. Kim, R. A. King, P. Klunzinger, D. Kosenkov, T. Kowalczyk, C. M. Krauter, K. U. Lao, A. D. Laurent, K. V. Lawler, S. V. Levchenko, C. Y. Lin, F. Liu, E. Livshits, R. C. Lochan, A. Luenser, P. Manohar, S. F. Manzer, S.-P. Mao, N. Mardirossian, A. V. Marenich, S. A. Maurer, N. J. Mayhall, E. Neuscamman, C. M. Oana, R. Olivares-Amaya, D. P. O'Neill, J. A. Parkhill, T. M. Perrine, R. Peverati, A. Prociuk, D. R. Rehn, E. Rosta, N. J. Russ, S. M. Sharada, S. Sharma, D. W. Small, A. Sodt, T. Stein, D. Stück, Y.-C. Su, A. J. W. Thom, T. Tsuchimochi, V. Vanovschi, L. Vogt, O. Vydrov, T. Wang, M. A. Watson, J. Wenzel, A. White, C. F. Williams, J. Yang, S. Yeganeh, S. R. Yost, Z.-Q. You, I. Y. Zhang, X. Zhang, Y. Zhao, B. R. Brooks, G. K. L. Chan, D. M. Chipman, C. J. Cramer, W. A. Goddard, M. S. Gordon, W. J. Hehre, A. Klamt, H. F. Schaefer, M. W. Schmidt, C. D. Sherrill, D. G. Truhlar, A. Warshel, X. Xu, A. Aspuru-Guzik, R. Baer, A. T. Bell, N. A. Besley, J.-D. Chai, A. Dreuw, B. D. Dunietz, T. R. Furlani, S. R. Gwaltney, C.-P. Hsu, Y. Jung, J. Kong, D. S. Lambrecht, W. Liang, C. Ochsenfeld, V. A. Rassolov, L. V. Slipchenko, J. E. Subotnik, T. Van Voorhis, J. M. Herbert, A. I. Krylov, P. M. W. Gill, M. Head-Gordon, *Mol. Phys.* **2015**, *113*, 184–215.

Entry for the Table of Contents



A dimethyldihydropyrene photochromic unit bearing electron-donor and -acceptor substituents has been synthesized and investigated by spectroscopy, electrochemistry and theoretical calculations (spin-flip TD-DFT). This system can be reversibly isomerized with very good quantum yields to its corresponding cyclophanediene form when irradiated by red light under inert atmosphere and is able to generate two endoperoxide isomers upon illumination under air. These endoperoxides can thermally release singlet oxygen.

Institute and/or researcher Twitter usernames: @DCMGrenoble ; @GuyRoyal3 ; @ZianiZakaria7